Journal of Neuroinflammation

RESEARCH

Open Access

Endothelial TREM-1 mediates sepsis-induced blood–brain barrier disruption and cognitive impairment via the PI3K/Akt pathway

Yuwen Su[1,2†], Wanwan Zhu[1,2†], Tong Su[1,2], Lian Huang[1,2], Mubing Qin[3], Qingyu Wang[1,2], Qi Xu[1,2*], Yi Li[3*] and Jianbo Xiu[1,2,4*]

Abstract

The blood–brain barrier (BBB) is a critical selective interface between the central nervous system (CNS) and the blood circulation. BBB dysfunction plays an important role in the neurological damage caused by sepsis. However, the mechanisms underlying the disruption of the BBB during sepsis remain unclear. We established a human induced pluripotent stem cell (iPSC)-derived BBB model and reported that treating with sepsis patient serum leads to structural and functional disruption of the BBB. In a cecal ligation and puncture (CLP)-induced mouse model of sepsis, we also observed disruption of the BBB, inflammation in the brain, and impairments in cognition. In both models, we found that the expression of TREM-1 was significantly increased in endothelial cells. TREM-1 knockout specifically in endothelial cells alleviated BBB dysfunction and cognitive impairments. Further study revealed that TREM-1 affects the expression of genes involved in the PI3K/Akt signaling pathway. The protective effects of TREM-1 inhibition on the BBB and cognition were abrogated by PI3K inhibitors. Our findings suggest that endothelial TREM-1 induces sepsis-induced BBB disruption and cognitive impairments via the PI3K/Akt signaling pathway. Targeting endothelial TREM-1 or the PI3K/Akt signaling pathway may be a promising strategy to maintain BBB integrity and improve cognitive function in sepsis patients.

Keywords Sepsis, Blood–brain barrier, Cognitive impairment, TREM-1, PI3K/Akt

†Yuwen Su and Wanwan Zhu have contributed equally to this work.

*Correspondence:
Qi Xu
xuqi@pumc.edu.cn
Yi Li
billliyi@126.com
Jianbo Xiu
xiujianbo@ibms.cams.cn
[1]State Key Laboratory of Common Mechanism Research for Major Diseases, Institute of Basic Medical Sciences, School of Basic Medicine Peking Union Medical College, Chinese Academy of Medical Sciences, Beijing 100005, China
[2]Neuroscience Center, Chinese Academy of Medical Sciences, Beijing 100005, China
[3]Emergency Department, The State Key Laboratory of Complex, Severe and Rare Diseases, Peking Union Medical College Hospital, Chinese Academy of Medical Science and Peking Union Medical College, Beijing 100730, China
[4]State Key Laboratory of Complex, Severe, and Rare Diseases, Beijing 100005, China

Introduction

Sepsis is a life-threatening multiorgan dysfunction syndrome caused by the host's overactive immune response to pathogenic infections [1]. More than half of all deaths in intensive care units are caused by sepsis, and sepsis is the leading cause of death in noncardiac patients in intensive care units. Although progress has been made in the diagnosis and management of clinical sepsis, morbidity and mortality remain high. Preliminary extrapolations based on data from high-income countries suggest that, globally, there are an estimated 31.5 million cases of sepsis and 19.4 million cases of severe sepsis, with approximately 5.3 million deaths per year [2]. Sometimes, sepsis first affects the brain [3]. It usually induces diffuse cerebral dysfunction in the absence of direct central nervous system (CNS) infection. Sepsis-associated encephalopathy (SAE) clinically manifests as acute brain damage and is characterized by delirium, cognitive impairment and even coma [4]. At present, sepsis symptoms are treated with anti-infective medications and supportive care; however, there are currently no treatments available that can effectively treat septic brain injury [5]. Additionally, despite the multiple serious consequences of sepsis, the underlying mechanism remains elusive, and there is no effective clinical treatment. The pathophysiology may involve neurotransmitter dysfunction, brain inflammation, ischemic lesions, microglial activation, and blood–brain barrier dysfunction [6].

Despite the incomplete elucidation of the pathological mechanisms underlying sepsis, several studies have demonstrated that blood–brain barrier dysfunction significantly contributes to sepsis-induced neurological impairment [7, 8]. The intact blood–brain barrier is the critical selective interface between the CNS and blood circulation [9]. The main component of the blood–brain barrier is cerebral microvascular endothelial cells, which together with astrocytes, pericytes, and other supporting cells, form neurovascular units [10–12]. Changes in the structure and function of the blood–brain barrier may be the key pathological mechanism of SAE. Maintaining blood–brain barrier integrity is an important strategy for the treatment of brain dysfunction in sepsis patients [13, 14]. The autopsy results of adult patients who died from sepsis revealed that brain barrier damage was associated with severe organ dysfunction and systemic inflammation [15]. Additionally, in animal models of sepsis, BBB disruption is always accompanied by neuroinflammation, which is manifested by the activation and proliferation of microglia in brain tissue and the elevation of proinflammatory cytokine levels [16].

Triggering receptor expressed on myeloid cell-1 (TREM-1) is an immune receptor that plays a key role in amplifying the inflammatory response [17, 18]. Trem1 is expressed in different cell types, such as neutrophils, natural killer cells, macrophages, endothelial cells, and platelets [18–20]. Amplification of the inflammatory response by TREM-1 is also currently recognized as a key factor in the dysregulation of the immune response in sepsis. Studies have shown that TREM-1 expression on immune cells is elevated in patients with sepsis and is associated with increased mortality [21]. Modulation of TREM-1 expression has proven to be a promising therapeutic strategy that could be used to develop new drugs and treatments for sepsis [21]. The PI3K/AKT pathway, according to previous research, is a conserved family of signal transduction enzymes that are able to coordinate a variety of intracellular signals, control cellular responses to external stimuli, and regulate cell survival and proliferation [22]. Previous studies have shown that PI3K/Akt signaling has anti-neuroinflammatory, antioxidative stress, and anti-apoptosis properties in neurons [23]. Studies have shown that the PI3K/Akt axis is downstream of TREM-1 and is involved in TREM-1-mediated inflammation [24]. However, the role of TREM-1 and its downstream PI3K/Akt pathway in the neuroinflammatory response to sepsis is still not fully understood.

In this study, we constructed a human-induced pluripotent stem cell (hiPSC)-induced BBB model and simulated BBB disruption by treating the cells with plasma from septic patients. In addition, cecal ligation and puncture (CLP) was performed in a mouse model to mimic the development of sepsis. We found that sepsis led to BBB disruption and cognitive impairment in mice and that TREM-1 was involved in this process. A protective effect of TREM-1 inhibition on the BBB and brain function was found via the knockdown or knockout of TREM-1 in endothelial cells. We then investigated the role of the PI3K/Akt pathway in the cerebral protective effect of TREM-1 inhibition using a PI3K inhibitor. Our study suggests that TREM-1 can affect BBB disruption and cognitive impairment in sepsis and that the PI3K/Akt pathway is involved in the neuroprotective effect of TREM-1 inhibition. These results suggest that TREM-1 inhibition may be a potential therapeutic approach for improving BBB integrity and promoting cognitive recovery in sepsis patients.

Materials and methods

Animals

Male mice were used in this study unless otherwise noted. Adult C57BL/6J mice aged 8 weeks were purchased from SPF (Beijing) Biotechnology Co., Ltd. Mice were housed in groups under a 12-h light/dark cycle. The mice were provided unrestricted access to water and food unless specific experimental requirements were met. All animals were raised and handled in accordance with the protocol approved by the institutional review board of the IBMS & Peking Union Medical College and were

conducted according to the Beijing Administration Office of Laboratory Animals guidelines for the care and use of laboratory animals.

Dermal fibroblast reprogramming and cell culture

Skin tissue was obtained from normal people and cultured with fibroblast medium consisting of high-glucose DMEM (Gibco), 20% fetal bovine serum (Gibco), 1% penicillin–streptomycin (MACGEN), 1% GlutaMax™ (Gibco), 1% nonessential amino acids (Gibco), and 0.1% β-ME (Gibco). After isolation from the tissue, fibroblasts at passage 2 were transduced with Sendai virus using the CytoTune™-ips2.0 Sendai Reprogramming Kit (Invitrogen, Cat. #A16517) according to the manufacturer's instructions. The collected iPSCs were cultured in a 6-well plate precoated with vitronectin (Gibco, Cat. #A31804). The cells were cultured with mTeSRTM Plus Medium (STEMCELL Technologies, Cat. #100–0276) at 37 °C and 5% CO2. The cells were passaged at a ratio of 1:6 every 3–4 days with a GCDR (STEMCELL Technologies, Cat. #100–0485) survival promoter.

Differentiation of iPSCs into endothelial cells

iPSC differentiation into endothelial cells was performed using a STEMdiff Endothelial Differentiation Kit (STEMCELL Technologies, Cat. #08005) according to the manufacturer's instructions. Specifically, iPSCs were seeded at a density of 7500 cells/cm2 in mTeSR™ Plus Medium + 10 μM Y-27,632 (STEMCELL Technologies, Cat. #72302) on a Matrigel®-coated 6-well plate. Twenty-four hours after seeding, the cells were cultured in STEMdiff™ Mesoderm Induction Medium (STEMCELL Technologies, Cat. #05002) for 48 h and then in STEMdiff™ Endothelial Induction Medium (STEMCELL Technologies, Cat. #08006). Four days later, the cells were harvested using Accutane (STEMCELL Technologies, Cat. #07920) and seeded in a STEMdiff™ Endothelial Expansion.

Differentiation of iPSCs into neural progenitor cells (NPCs) and induction of astrocyte differentiation

iPSCs were seeded at a density of 2×10^5 cells/cm^2 in SMADi Neural Induction Medium + 10 μM Y-27,632 on a Matrigel®-coated 6-well plate. After 24 h, the medium was changed to the STEMdiffTM SMADi Neuronal Induction Kit (STEMCELL Technologies), and the medium was changed daily. On day 8, the cells were resuspended at a density of 2×10^5 cells/cm^2 in Matrigel-coated 6-well plates. The procedure was repeated twice. After the third passage, the medium was changed to STEMdiffTM Neural Progenitor medium, and the medium was changed daily.

NPCs were collected using Accutase and seeded in neural induction medium on a Matrigel-coated 6-well plate. After 24 h, the medium was changed to astrocyte differentiation medium, and the medium was changed daily. The procedure was repeated twice. After the third passage, the medium was changed to astrocyte maturation medium. After 2–3 passages of cell culture, mature astrocytes were observed.

Differentiation of iPSCs into pericytes

iPSCs were differentiated into pericytes by adapting previously published protocols [25, 26]. iPSCs were seeded at a density of 5×10^4 cells/cm^2 in mTeSR™ Plus Medium + 10 μM Y-27,632 on a Matrigel®-coated 6-well plate. After 24 h, the medium was changed to STEMdiff™ Mesoderm Induction Medium. The medium was changed daily for 5 days for mesoderm induction. The cells were seeded at a density of 2.5×10^4 cells/cm^2 on a Matrigel-coated 6-well plate and maintained in Pericyte Medium (ScienCell, Cat. #1201).

Construction of the BBB cell model

A triple culture model of the BBB was constructed. First, pericytes were cultured on the underside of the inserts of a Matrigel-precoated Transwell system. Twelve hours later, astrocytes were cultured in the same manner on the underside of the inserts. After 12 h, the Transwell apparatus was turned, and endothelial cells were seeded on the semipermeable membrane of the insert.

Transwell TEER measurement

The TEER value of the BBB model was measured using EVOM2 (World Precision Instruments, Sarasota, FL, United States) every 24 h before the media were changed. Each Transwell insert was measured three times, and care was taken to measure quickly at room temperature to minimize temperature fluctuations. The actual resistance value was calculated as the resistance measurement minus the resistance value of the blank insert. Finally, this value was multiplied by the surface area of the Transwell membrane as the final resistance value, and the unit was $\Omega \cdot cm^2$.

FITC-dextran permeability detection

To test the permeability of the model, fluorescein isothiocyanate (FITC)-dextran was added to the upper chamber of the Transwell system for one hour. Samples were collected from the upper and lower chambers and analyzed for fluorescence. The fluorescence intensity was measured at 490/520 nm. The permeability was denoted by Pe and was calculated using the following equation: Pe (cm/s)=([A]/t)× (I/A)×(V/[L]). where [A] is the concentration of FITC-dextran in the lower chamber, t(s) is the time interval, A(cm2) is the Transwell membrane surface area, V(m3) is the volume of solution in the lower chamber, and [L] is the concentration of FITC-dextran in the upper chamber.

Establishment of the CLP model

The mice were deeply anesthetized, and the limbs were fixed. An incision of approximately 1 cm was made in the middle of the lower abdomen. The cecum was exposed, ligated at 50% using 3.0 silk, and punctured twice using a 21-gauge needle. The fecal contents were then extruded by squeezing the cecum. The intestinal tract was relocated to the abdominal cavity. The abdomen was closed. Sterile saline solution (37 °C) was subcutaneously injected for fluid resuscitation. The mice in the sham group underwent the same operation procedure but without ligation or puncture.

Lentiviral vector construction and transduction

Lentiviral Vector Design: TREM-1 Knockdown (KD): Lentiviral vectors were constructed using the carrier element sequence *hU6-MCS-CBh-gcGFP-IRES-puromycin*. A scrambled shRNA vector (*hU6-MCS-CBh-gcGFP-IRES-puromycin*) served as the negative control. TREM-1 Overexpression (OE): The overexpression vector utilized the sequence *Ubi-MCS-3FLAG-CBh-gcGFP-IRES-puromycin*, with an empty vector (*Ubi-MCS-3FLAG-CBh-gcGFP-IRES-puromycin*) as the control.

Viral Transduction: Cells were transduced with lentivirus at a multiplicity of infection of 50 for 72 h. Transduction efficiency was confirmed via GFP fluorescence.

rAAV packaging and tail vein injection

rAAVs were packaged by Brain Case, China, and include: rAAV-nEF1a-spCas9-SV40 NLS-3xHA-polyA, rAAV-CMV-EGFP-bGH polyA-U6-SpsgRNA1(mTrem1). Mice were injected with virus by tail vein injection. rAAV was injected in 10^{11} vector genome (v. g.).

Assessment of BBB integrity by Evans blue extravasation

The mice were injected with 2% Evans blue (4 mL/kg body weight) via the tail vein 2 h prior to sacrifice. The mice were anesthetized and then perfused with ice-cold normal saline to remove dye from the blood vessels. Brain samples were collected, weighed, and then homogenized in formamide at 60 °C for 18 h. The concentration of infiltrated Evans blue was quantified at 620 nm using a multimode microplate reader (BioTek Synergy H1). The data are presented as nanograms per gram of brain weight.

Isolation of mouse brain endothelial cells

The procedure begins with anesthesia and PBS perfusion of the mouse, followed by brain extraction on ice and coronal sectioning. Tissue sections are digested using a dissociation buffer and processed in a tissue dissociator for 15 min (mouse brain program). The resulting suspension is filtered through a 70 μm strainer, washed with DPBS, and centrifuged (300 g, 4 °C, 10 min). After removing debris via gradient centrifugation with a debris removal reagent (layered with DPBS, 3000 g, 4 °C, 10 min), cells undergo sequential magnetic sorting: first, CD45-negative selection to deplete immune cells using magnetic beads (15 min incubation, 4 °C, protected from light), followed by CD31-positive selection to enrich endothelial cells under identical conditions. Purified cells are washed with DPBS/BSA buffer, and viability is assessed by mixing the suspension 1:1 with AO/PI stain for automated cell counter analysis. Critical steps include maintaining low-temperature operations, dual magnetic bead-based purification (CD45−/CD31+), and gradient centrifugation for debris removal to ensure high-purity endothelial cell isolation.

Isolation of RNA and real-time quantitative PCR (RT–qPCR)

Total RNA was extracted from cells or tissues using TRIzol reagent (Invitrogen, California, USA). The concentration and purity of the RNA were determined by spectrophotometry at a ratio of 260:280. Total RNA was reverse transcribed using a Transcriptor First Strand cDNA Synthesis Kit (04897030001, Roche). The expression levels of mRNA were assessed with real-time PCR by using FastStart Essential DNA Green Master Mix (06924204001; Roche). A fragment of GAPDH was amplified as the internal control. All reactions were run on a Roche LightCycler 96 real-time PCR instrument. The data were analyzed using the comparative Ct method. All primer sequences are listed in Table S1.

Protein electrophoresis and Western blotting

The cells or tissues were ultrasonically lysed in CelLytic M (Sigma–Aldrich, Cat. # C2978) supplemented with a protease inhibitor cocktail (Bimake, Cat. # B14002). A Pierce BCA protein assay (Thermo Fisher, Cat. #23225) was used to determine the protein concentration. Protein samples were loaded onto SDS–polyacrylamide gels and transferred to nitrocellulose membranes. The membranes were blocked with nonfat milk solution (5%) at room temperature for 1 h and incubated overnight at 4 °C with the primary antibody probe (listed in Table S2). The membranes were incubated with the corresponding HRP-conjugated secondary antibodies (listed in Table S2) at room temperature for 1 h. Target protein levels were analyzed via ImageJ and normalized to those of GAPDH or β-actin.

Enzyme-linked immunosorbent assay (ELISA)

To measure the levels of chemokines released from the cell cultures, the supernatants were collected and centrifuged at 5,000 × g for 10 min. IL-6 and IL-1β levels were measured with an ELISA kit according to the manufacturer's protocols.

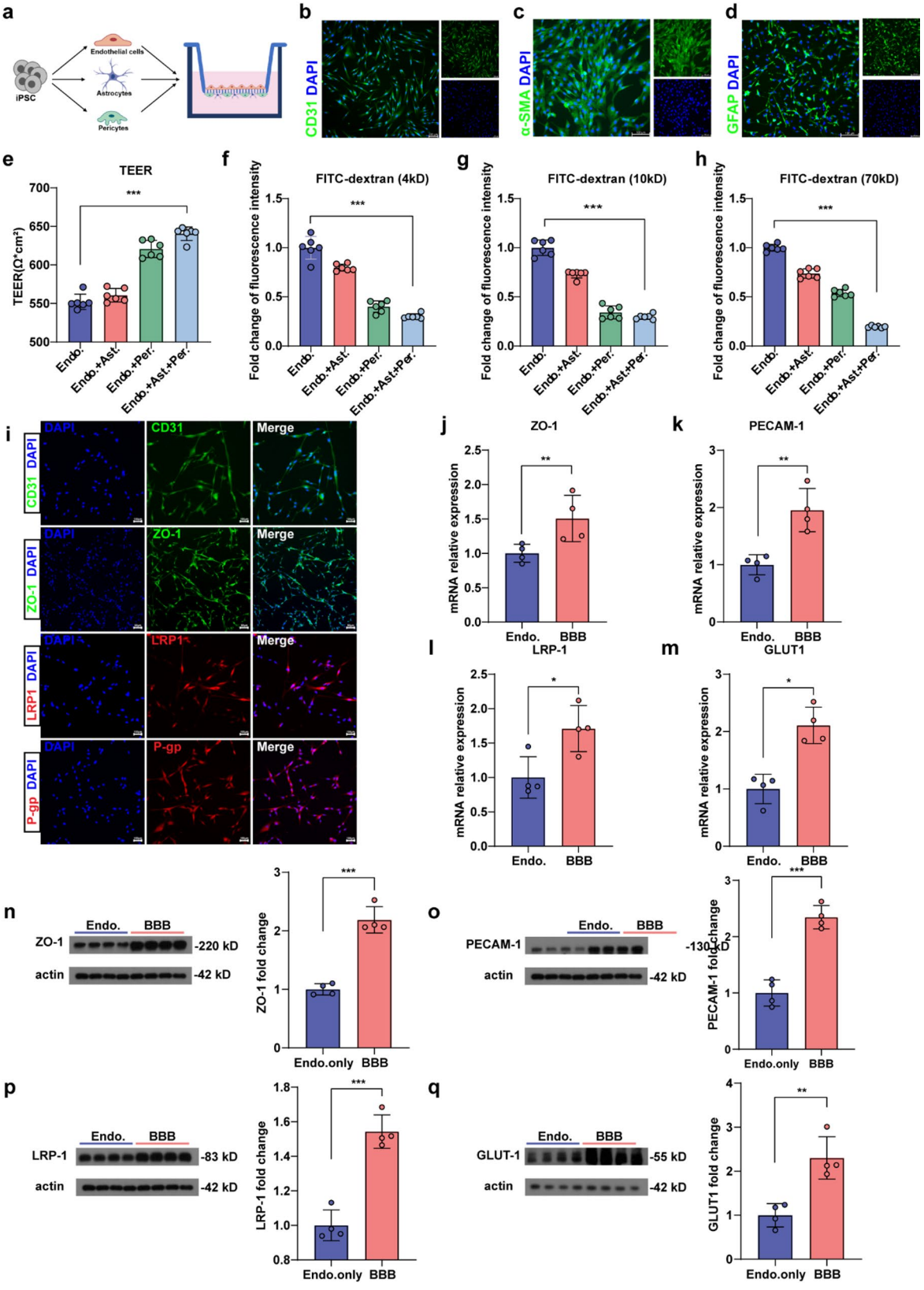

Fig. 1 (See legend on next page.)

(See figure on previous page.)

Fig. 1 Reconstruction of the structure and physiological properties of the BBB in vitro. **a**, Schematic diagram showing the establishment of the iPSC-derived BBB in vitro model. **b**, iPSC-derived endothelial cells stained with CD31. **c**, iPSC-derived pericytes stained for α-SMA. **d**, iPSC-derived astrocytes stained with GFAP. **e**, TEER measurements of iPSC-derived endothelial cells, iPSC-derived endothelial cells plus astrocytes, iPSC-derived endothelial cells plus pericytes, and the BBB model in vitro. **f**-**h**, Permeability of endothelial cells alone, endothelial cells plus astrocytes, endothelial cells plus pericytes, or the BBB model to fluorescently-labeled dextran (4kD, 10kD, 70kD) in vitro. **i**, BBB model endothelial cells stained with ZO-1, PECAM-1, LRP-1, and GLUT1. **j**-**m**, RT–qPCR analysis of the expression levels of ZO-1, PECAM-1, LRP-1, and GLUT1. **n**-**q**, Western blot analysis of ZO-1, PECAM-1, LRP-1, and GLUT1 protein expression. $n = 6$ per group for e-h. $n = 4$ per group for j-q. White scale bar: 100 μm. The data are presented as the means ± SEMs. ns, not significant, $^{*}P < 0.05$, $^{**}P < 0.01$, $^{***}P < 0.001$, Student's t test

Neurobehavioral scores

After CLP, the neurobehavioral scores were used to evaluate the neurobehavioral changes in the mice according to the corneal reflex, auricular reflex, tail flick reflex, righting reflex, and avoidance reflex. Corneal reflex: the cornea was gently touched with a cotton swab to observe whether the mouse blinked or shook its head. Auricular reflex: the mouse auricle was touched to observe whether the mouse turned its head. Tail flick reflex: the mouse's tail was stimulated to see if the mouse would run away. Righting reflex and avoidance reflex: the mice were placed in the supine position, and whether the mice switched to the prone position with their feet on the ground was observed. Two points were given if the mouse responded normally. If the mouse was hyperreflexia (lacking a reflex for 10 s), 1 point was given. A score of 0 was given if the mouse had no reflex. The final neurobehavioral score was the total score of the above five items.

Morris water maze (MWM) test

Spatial memory was evaluated using the MWM test [27], which began on the sixth postoperative day. During the training phase, the mice located the hidden underwater platform using four visual cues on the pool wall for 4 consecutive days. For each trial, the mice had a maximum of 60 s of swimming time. The experiment ended when the mice swam on the platform or when the time reached 60 s. After resting on the platform for 10 s, the mice were returned to their cages and allowed to dry. The escape latency was the time taken for the mice to reach the platform. On the fifth day of the MWM test, the platform was removed, and a trial lasting 60 s was conducted. The movement trajectories of the mice were recorded during the experiment. The swimming time of the mice in the target quadrant and the number of times the mice crossed the original platform location were recorded.

Novel object recognition test

The novel object recognition test is a relatively fast and efficient way to test learning and memory in mice. This experimental procedure was performed according to a previously reported protocol with some modifications [28]. The experimental procedure consisted of three phases: habituation, training, and testing. The mice were placed in the experimental apparatus (no object) to explore freely for 10 min. The next day, two identical objects, free of any animal scents and difficult to move, were placed into the device, and the mice were allowed to explore freely for 10 min. On the third day, an old object was replaced with a new object, and the mice were allowed to explore the object for 5 min. The exploration of the mice in each experiment was recorded. The recognition index was calculated for each animal.Recognition index= number of explorations of novel object / (number of explorations of novel object + number of explorations of familiar object)

LY294002 administration method

LY294002 is a broad-spectrum PI3K inhibitor. For cell experiments, cells were treated with LY294002 at a concentration of 50μM for 24 h. LY294002 was administered at a dose of 50 mg/kg via the tail vein to mice with treatment duration (3 days prior to sepsis induction).

Statistical analysis

All statistical analyses were conducted using GraphPad Prism software (Version 8.3.0), with quantitative data expressed as mean ± SEM, where *n* represents the number of biologically independent replicates. Normality of distribution was first assessed via the Shapiro-Wilk test ($\alpha = 0.05$). For datasets violating normality assumptions, non-parametric analyses were applied: Mann-Whitney U tests for two-group comparisons and Kruskal-Wallis tests with Dunn's post hoc correction for three or more groups. Normally distributed data underwent parametric testing, utilizing unpaired two-tailed t-tests (with Welch's correction for unequal variances) for two-group comparisons, while one-way ANOVA followed by Tukey's honestly significant difference (HSD) post hoc test was employed for multi-group analyses to rigorously control type I error rates. Statistical significance thresholds were defined as $^{*}p < 0.05$, $^{**}p < 0.01$, $^{***}p < 0.001$, $^{****}p < 0.0001$.

Results

Establishment of a human iPSC-derived BBB model

To investigate the molecular mechanisms by which sepsis affects the BBB, we established an in vitro BBB model employing human iPSCs. The formation of the human BBB involves interactions among three distinct cell types: brain endothelial cells, pericytes, and astrocytes [29, 30]. We first defined a protocol for constructing an in vitro BBB cell model (Fig. 1a). We used human iPSCs

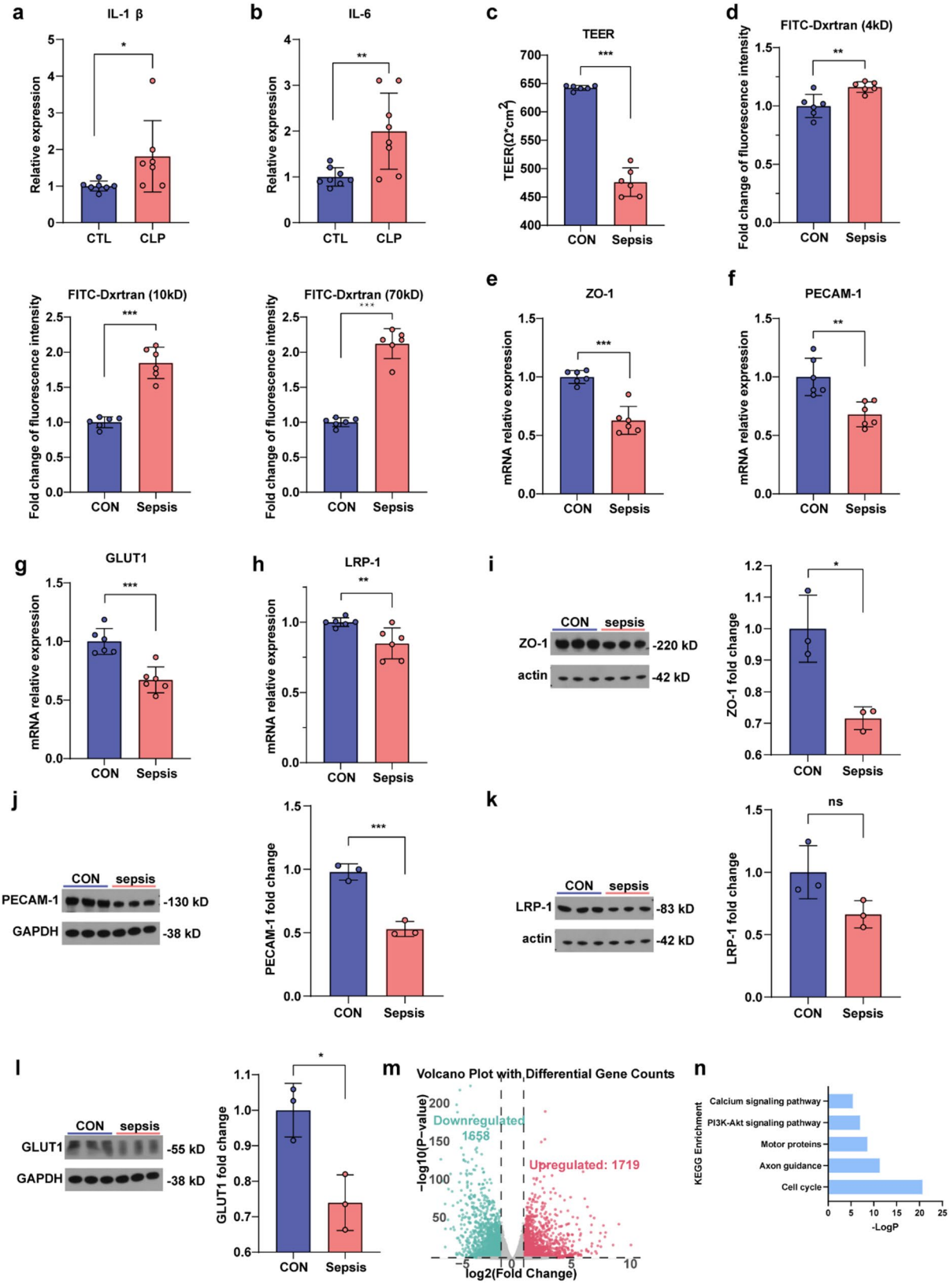

Fig. 2 (See legend on next page.)

(See figure on previous page.)

Fig. 2 Sepsis disrupts the structure and function of the BBB in an in vitro BBB model. **a**, ELISA of the expression level of the proinflammatory factor IL-1β in the serum of normal individuals or patients with sepsis. **b**, ELISA of the expression level of the proinflammatory factor IL-6 in the serum of normal individuals or patients with sepsis. **c**, TEER values of the BBB model treated with normal or septic serum. **d**, Permeability of endothelial cells alone, endothelial cells plus astrocytes, endothelial cells plus pericytes, or the blood-brain barrier to fluorescently labeled dextran in vitro. **e**-**h**, RT–qPCR analysis of the expression levels of *Zo-1*, *Pecam-1*, *Lrp-1*, and *Glut1*. **i**-**l**, Western blot analysis of ZO-1, PECAM-1, LRP-1, and GLUT1 protein expression. **m**, Volcano plot for differential expression analysis between endothelial cells after adding serum from patients with sepsis or normal human serum. **n**, Kyoto Encyclopedia of Genes and Genomes (KEGG) enrichment analysis of the differentially expressed genes. $n = 7$ per group for **a**. $n = 8$ per group for **b**. $n = 6$ per group for **c**-**h**. $n = 3$ per group for **i**-**l**. The data are presented as the means ± SEM. ns, not significant, $^{*}P < 0.05$, $^{**}P < 0.01$, $^{***}P < 0.001$, Student's t test

to induce the differentiation of endothelial cells, astrocytes, and pericytes, and established the model using a Transwell system. Endothelial cells were seeded in the chamber above the permeable Transwell membrane, and astrocytes and pericytes were placed on the back side of the membrane. Immunofluorescence staining was performed to validate the successful differentiation of iPSCs into endothelial cells, pericytes, and astrocytes. Endothelial cells expressed the endothelial marker CD31 (Fig. 1b), pericytes expressed α-SMA (Fig. 1c), and astrocytes expressed GFAP (Fig. 1d). Transepithelial/transendothelial electrical resistance (TEER) is a powerful indicator of cell barrier integrity and can be performed without causing cell damage [31]. The monolayer of endothelial cells in our Transwell system had a TEER value of approximately 550 $\Omega \cdot cm^2$, and the TEER value increased when the cells were cocultured with astrocytes or pericytes. When endothelial cells, astrocytes, and pericytes were cultured together, the TEER value was the highest, nearly 650 $\Omega \cdot cm^2$, indicating that the barrier integrity was greater in the coculture model than the other models (Fig. 1e). Next, we compared the molecular permeability of the BBB model. Compared with that in endothelial monolayers, the permeability of 4 kDa molecules in the BBB coculture model was reduced by approximately 70% (Fig. 1f). The permeability of Dextrans with larger molecular weights (10 kDa and 70 kDa) was also reduced in the BBB model than the endothelial monocultures, especially that of 70 kDa molecules, which was reduced by 80% (Fig. 1g-h), indicating that the BBB model exhibited lower permeability.

The low paracellular permeability of the BBB is due mainly to the tight junctions between endothelial cells, which are composed of the proteins zonula occludens-1 (zo-1) and platelet endothelial cell adhesion molecule-1 (PECAM-1) [32]. Moreover, the expression of receptors such as the glucose transporter type 1 (GLUT-1) and the low-density lipoprotein receptor–related protein-1 (LRP-1) is an important feature of the BBB and helps mediate the crossing of substances across the barrier [33]. Immunofluorescence staining confirmed the expression of BBB-associated proteins ZO-1, PECAM-1, LRP-1, and GLUT1 in our in vitro cell-based BBB model (Fig. 1i). Finally, we examined the expression levels of genes involved in maintaining the structure and function of the BBB by a quantitative real-time PCR (qRT−PCR) assay in endothelial cells cultured alone or in coculture with astrocytes and pericytes. Compared with that in endothelial cells cultured alone, the expression of the BBB-related genes *Zo-1*, *Pecam-1*, *Lrp-1*, and *Glut1* was significantly increased in endothelial cells in the BBB model (Fig. 1j−m). Moreover, the Western blot results confirmed that the expression of the BBB-related proteins ZO-1, PECAM1, LRP-1, and GLUT1 was increased in cocultured endothelial cells (Fig. 1n-q).

Serum from sepsis patients disrupts the structure and function of the human iPSC-derived BBB model

Next, we investigated the impact of serum from sepsis patients on the structure and function of the BBB model. First, we examined the serum levels of IL-1β and IL-6, which are often elevated in sepsis [34, 35]. Our results revealed that the serum levels of these two inflammatory factors increased significantly, indicating that peripheral inflammation occurred in patients with sepsis (Fig. 2a, b). Next, we determined the optimal timing and concentration of serum applied to the BBB model by examining the barrier integrity of the model. When the serum concentration was 20%, the model had the lowest TEER values and the highest permeability at 48 h, indicating that the serum at high concentrations had the most destructive effect on the model (Fig. S1). When the BBB model was treated with serum from sepsis patients, the TEER value was significantly lower, indicating that the barrier integrity of the cell layer was reduced (Fig. 2c). Moreover, the permeability of the model was examined. The permeability of the BBB model to 4 kDa, 10 kDa, and 70 kDa dextran increased, especially that of macromolecular dextran (Fig. 2d), which further suggested that the integrity of the BBB model was disrupted. We subsequently performed qRT−PCR analysis of endothelial cells in the model. We found that the expression of the BBB-related genes *Zo-1* (Fig. 2e) and *Pecam1* (Fig. 2f) in endothelial cells decreased after the addition of serum from sepsis patients, indicating that the structure of the BBB was destroyed. In addition, the expression of *Glut1* and *Lrp-1* decreased (Fig. 2g, h), indicating that the function of the blood-brain barrier may be disrupted. Western blot analysis revealed that the expression of the BBB-related proteins ZO-1, PECAM-1, and GLUT1 was decreased, whereas LRP-1 expression was not significantly changed (Fig. 2i−l). Our study demonstrated that the addition of

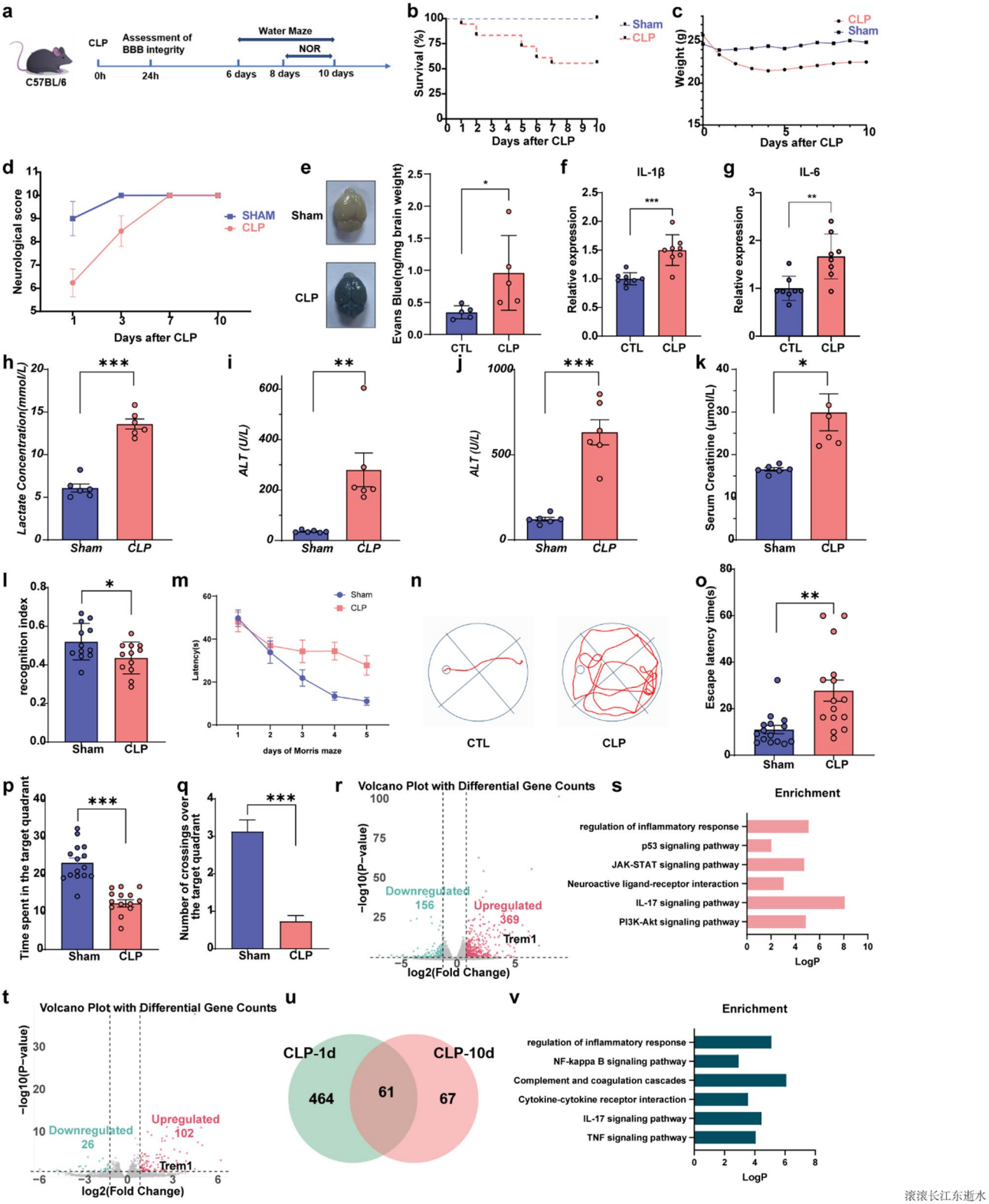

滚滚长江东逝水

Fig. 3 (See legend on next page.)

(See figure on previous page.)

Fig. 3 Sepsis induced by CLP surgery leads to BBB barrier disruption and brain function impairment. **a**, Schematic illustration of the experimental design. **b**-**c**, Mortality and changes in body weight of the mice in the sham ($n=12$ mice) and CLP ($n=20$ mice) groups within 10 days after the operation. **d**, Neurobehavioral scores of the mice in the sham and CLP groups within 10 days after surgery. **e**, Representative brain images showing CLP surgery-induced Evans blue leakage and its quantification, expressed as nanograms of dye per gram of brain weight (ng/mg), $n=5$ per group. **f**-**g**, ELISA of the expression level of the proinflammatory factor IL-1β and IL-6 in the hippocampi, $n=8$ per group. **h**-**k**, Serum lactate concentration (mmol/L), ALT (U/L), AST (U/L), and Serum creatinine (μmol/L) levels measured 24 h after sham or CLP surgery, $n=6$ per group. **l**, Recognition indices of the mice in the sham and CLP groups, $n=12$ per group. **m**, Latency time of mice in the sham and CLP groups. **n**, Representative images of the trajectories of the mice in the MWM test. **o**-**q**, Latency, duration of stay in the target quadrant, and number of crossing platform locations in sham and CLP groups of mice. $n=15$ per group for **m**, **o**-**q**. The data are presented as the means ± SEM. ns, not significant, $^{*}P<0.05$, $^{**}P<0.01$, $^{***}P<0.001$, Student's t test. **r**, Volcano plot of differentially expressed genes between the CLP-1 day group and the sham group. **s**, KEGG enrichment analysis of the differentially expressed genes between the CLP-1 day group and the sham group. **t**, Volcano plot of differentially expressed genes between the CLP-10 day group and the sham group. **u**, Venn diagram showing the number of changes in the transcriptional profile of mouse brain endothelial cells at 1 and 10 d after CLP. **v**, KEGG enrichment analysis of the genes with consistent expression in mouse endothelial cells on day 1 and day 10 after CLP

serum from patients with sepsis to the BBB cell model resulted in decreased integrity and increased permeability of the BBB, as well as reduced expression levels of several BBB-related genes and proteins, indicating that the structure and function of the BBB are disrupted during sepsis. Next, we performed transcriptional profiling by RNA sequencing of endothelial cells isolated from BBB models treated with normal human or septic serum. A total of 1719 upregulated genes and 1658 downregulated genes were identified (Fig. 2m). Further pathway enrichment analysis of the differentially expressed genes revealed that calcium signaling pathway, PI3K/Akt pathway, etc. were enriched in the downregulated genes in the endothelial cells treated with sepsis patient serum (Fig. 2n).

Sepsis induced by CLP surgery leads to disruption of the BBB and cognitive impairment

Previous studies have revealed that sepsis model animals present brain inflammation and that the BBB is compromised in the CLP animal model [36, 37]. Our study confirmed the occurrence of brain inflammation and disruption of the BBB in adult male C57BL/6J wild-type (WT) mice subjected to CLP surgery. In this study, the CLP procedure was used to induce sepsis in model mice (Fig. 3a). All of the sham mice appeared to be normal, with 100% survival, whereas the septic mice died after CLP, with a final survival rate of 60% (12 of 20 mice survived) (Fig. 3b). Compared with the relatively stable weight of the sham mice, the surviving mice after CLP surgery presented significant weight loss (Fig. 3c). In addition, diarrhea, pyuria, closed eyes or eye secretions, reduced movement and other phenomena were observed in the CLP-induced sepsis model mice.

To assess the behaviors of the mice, we used neurobehavioral scores to evaluate the neurobehavioral changes in the mice, including the corneal reflex, righting reflex, auricle reflex, tail flick reflex, and avoidance reflex [38]. As shown in Fig. 3d, during our observation period, the mice in the CLP group performed poorly. In the first three days after surgery, the neurobehavioral scores of the CLP group were significantly lower than those of the sham group. One day after CLP surgery, we observed that sepsis triggered the loss of BBB integrity in the mice, as demonstrated by the results of the Evans blue extravasation experiment (Fig. 3e).

Considering that sepsis triggers a systemic inflammatory response that affects the brain [36], we then evaluated inflammation within brain tissue. We found that, 24 h after the onset of sepsis, IL-1β (Fig. 3f) and IL-6 (Fig. 3g) levels were increased in the hippocampi of the mice in the CLP group compared with the sham group. In the CLP-induced sepsis mouse model, significant elevations in four critical biomarkers were observed 24 h post-surgery (Fig. 3h-k). Lactate, a marker of anaerobic metabolism and tissue hypoxia, showed increased serum levels, indicative of systemic hypoperfusion and metabolic acidosis. Both alanine aminotransferase (ALT) and aspartate aminotransferase (AST), enzymes released during hepatocyte injury, demonstrated heightened activity, reflecting sepsis-associated liver dysfunction. Similarly, serum creatinine, a key indicator of renal filtration capacity, exhibited a marked rise, suggesting impaired glomerular filtration and acute kidney injury. These findings collectively highlight the development of multiorgan dysfunction, encompassing metabolic derangements, hepatic damage, and renal failure, in response to CLP-induced systemic inflammation.

Sepsis can lead to associated cognitive dysfunction [37], so we then performed behavioral tests on the mice one week after CLP surgery to observe their cognitive function (Fig. 3a). The results of the novel object recognition experiment revealed that the mice in the CLP group exhibited fewer explorations of the novel object, and the recognition index was significantly lower than that in the sham group (Fig. 3l). In the Morris water maze test, we measured the escape latency (Fig. 3m) and observed that mice in the CLP group traveled a significantly longer distance before locating the platform (Fig. 3n). Assessment of motor activity in the MWM test revealed a significant increase in the time to reach the platform in septic mice compared with the sham mice (Fig. 3o). We also found that CLP-treated mice spent less time in the target quadrant (Fig. 3p) and crossed the target quadrant

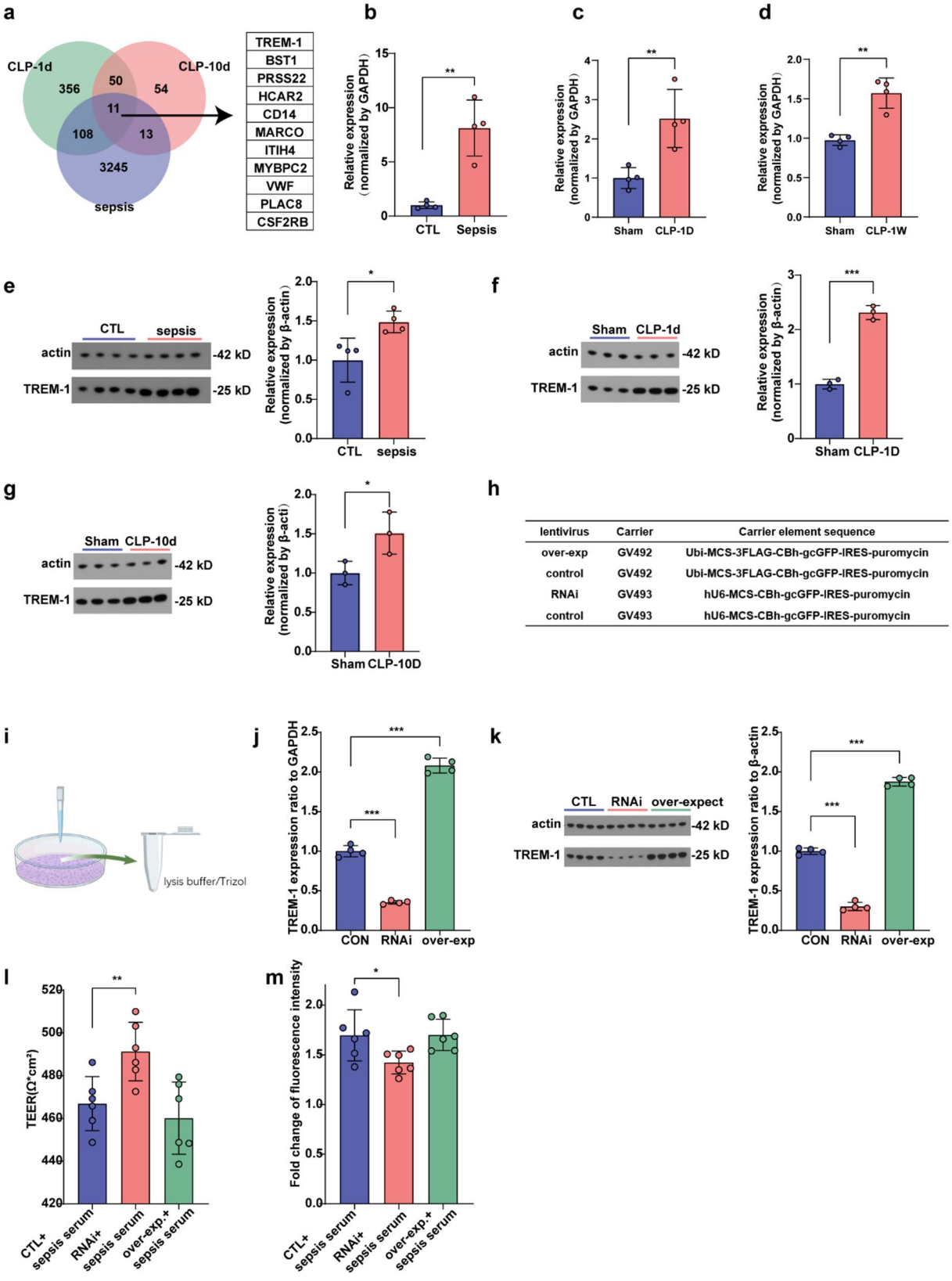

Fig. 4 (See legend on next page.)

(See figure on previous page.)

Fig. 4 Endothelial TREM1 is involved in BBB disruption. **a**, Venn diagram of changes in the transcriptional profiles of endothelial cells in cell models treated with serum from patients with sepsis and normal human serum in cell experiments and changes in the transcriptional profiles of mouse brain endothelial cells at 1 and 10 days after CLP. **b**, RT–qPCR analysis of TREM-1 expression in endothelial cells isolated from BBB models supplemented with normal human or septic serum. **c**-**d**, RT–qPCR analysis of the expression level of TREM-1 on day 1 and day10 after the operation in the sham operation group and the CLP group. **e**, Western blot analysis of TREM-1 expression in endothelial cells isolated from BBB models treated with normal human or septic serum. **f**-**g**, Western blot analysis of the expression level of TREM-1 on day 1 and day 10 after the operation in the sham operation group and the CLP group. **h**, Schematic representation of the lentiviral vector. **i**, Schematic of protein extraction from endothelial cells after virus injection. **j**-**k**, RT–qPCR analysis and western blot analysis of TREM-1 expression in endothelial cells with TREM-1 knockdown or overexpression. **l**, TEER of the BBB models constructed with normal, TREM-1-knockdown, or TREM-1-overexpressing endothelial cells after the addition of septic patient serum. **m**, Magnitude of increase in permeability of fluorescently labeled dextran (10 kDa) in the BBB models with normal, TREM-1-knockdown, or TREM-1-overexpressing endothelial cells after the addition of septic patient serum.$n = 4$ per group for b-e, j-k. $n = 3$ per group for f-g. $n = 6$ per group for l-m. The data are presented as the means ± SEM. ns, not significant, $^{*}P < 0.05$, $^{**}P < 0.01$, $^{***}P < 0.001$, b-g, Student's t test. j-m, One-way ANOVA

fewer times (Fig. 3q), suggesting that sepsis caused spatial memory dysfunction in these mice. In addition, we collected cerebral endothelial cells from mice at 24 h and 10 days after CLP and performed transcriptome sequencing. Compared with those in the sham group, 369 genes were upregulated and 156 genes were downregulated in the cerebral endothelial cells of mice at 1 day after CLP (Fig. 3r), and further pathway enrichment analysis of the differentially expressed genes suggesting several possible related pathways (Fig. 3s). Compared with those in the sham group, 102 genes were upregulated and 26 genes were downregulated in the cerebral endothelial cells of mice at 10 day after CLP (Fig. 3t). A total of 61 genes with consistent expression were identified by transcriptional profiling of mouse brain endothelial cells on days 1 and 10 after CLP (Fig. 3u). Further KEGG pathway analysis revealed enrichment of several pathways for consistently expressed genes (Fig. 3v).

Endothelial TREM1 is involved in BBB disruption in both the human iPSC-derived BBB model and the mouse CLP model

Next, we analyzed the results of previous experiments and evaluated the changes in the transcriptional profiles of endothelial cells in cell models treated with sepsis patient serum or normal human serum and the changes in the transcriptional profiles of mouse brain endothelial cells 1 day and 10 days after CLP surgery. Eleven genes, *Bst1*, *Prss22*, *Hcar2*, *Cd14*, *Marco*, *Trem1*, *Itih4*, *Mybpc2*, *Vwf*, *Plac8* and *Csf2rb*, were found to have consistent expression changes in the three groups (Fig. 4a). We subsequently used qPCR to examine gene expression in cell and animal samples and detected consistent expression of 5 genes, namely, *Marco*, *Trem1*, *Cd14*, *Hcar2* and *Mybpc2* (Fig. S2-4). Previous studies have shown that TREM-1 can amplify inflammation and cause functional damage to organs [39, 40]. Here, we hypothesize that TREM-1 is involved in BBB disruption in sepsis. First, we detected increased *TREM-1* gene expression in cell models supplemented with septic patients and in brain endothelial cells from mice 1 or 10 days after CLP surgery (Fig. 4b-d). The same phenomenon was also detected via Western blotting, and the protein expression level of TREM-1 was significantly increased (Fig. 4e-g). Next, we constructed TREM-1-knockdown or TREM-1-overexpressing lentiviruses (Fig. 4h), added them to the cell culture medium, and harvested endothelial cells after three days of treatment (Fig. 4i). Next, endothelial cells with TREM-1 knockdown or overexpression were generated via the addition of virus (Fig. 4j-k), and the TEER values and permeability were examined. In analyses of tightness and permeability, compared with normal endothelial cells, TREM-1-knockdown endothelial cells were found to be less responsive to septic serum, as indicated by a higher TEER value in the BBB model (Fig. 4l) and a lower increase in permeability to FITC−dextran (Fig. 4m). These findings suggest that TREM-1 knockdown, to a certain extent, hinders the destructive effect of serum from septic patients on BBB function.

TREM-1 knockout in endothelial cells alleviates cognitive impairment in a CLP mouse model

On the basis of the increased expression of TREM-1 in the brain endothelial cells of septic mice, we used AAV-BI30 as a gene transfer vector for endothelial expression of a single guide (sgRNA) against TREM-1 (Fig. 5a) to investigate the function of TREM-1 in sepsis. AAV-BI30 can achieve efficient and endothelial cell-specific Cre-mediated genetic modulation in the CNS [41]. Moreover, recombinant adeno-associated virus (rAAV), which we constructed, can target brain endothelial cells. One month after rAAV injection via the tail vein, TREM-1 was not expressed in the brain endothelial cells of the mice injected with TREM-1 sgRNA compared with those of the control mice (Fig. 5b). After rAAV injection, the mice were subjected to CLP surgery, and the antiseptic effect of TREM-1 knockout on the brain endothelial cells of CLP mice was evaluated by body weight assessment, neurobehavioral scoring, novel object recognition tests and MWM tests (Fig. 5c). The number of mouse deaths in each group was counted, and the mice in the sham operation group behaved normally, with a 100% survival rate. In the CLP group, the survival rate of the mice injected with the TREM-1 sgRNA was 63.6%, which was greater

than that of the control mice (55%) (Fig. 5d). In the body weight assessment, compared with the sham operation, the CLP surgery significantly reduced the body weights of the mice.While the difference was not statistically significant, TREM-1 knockout mice tended to recover body weight more rapidly than control mice (Fig. 5e). The neurobehavioral scores of the sham group returned to baseline immediately after a slight decrease on the first day after surgery. In the CLP group, the amplitude of the scores decreased on the first day after the operation and slowly returned to baseline at 1 week after the operation. Moreover, the neurobehavioral scores of the TREM-1 knockout mice returned to normal more rapidly than did those of the control mice at one week, although they also underwent CLP surgery (Fig. 5f). One day after CLP, we performed an Evans blue test to evaluate the permeability of the BBB in mice and found that TREM-1 knockout alleviated the BBB damage caused by CLP (Fig. 5g). Next, we examined whether TREM-1 knockout could alleviate cognitive impairment in sepsis. Behavioral tests were performed starting on day 6 after CLP. The recognition index, which is the frequency of exploration of the novel object by the mouse, was recorded in the novel object recognition test. Compared with control mice, TREM-1 knockout mice presented a higher recognition index after CLP (Fig. 5h). In the MWM experiment, the movement trajectory of the mice was recorded, along with the latency to reached the platform, the movement time in the target quadrant, and the number of times the mice crossed the target quadrant.The water maze test revealed that TREM1 knockout mice, although not different in terms of the latency to reach the platform on the last day, reached the platform in a shorter time during the first few days of training than did control mice, which also underwent CLP surgery (Fig. 5i, j). In addition, we found that TREM-1 knockout mice had longer movement times and more crossing times in the target quadrant than control mice did, indicating that TREM-1 knockout alleviated cognitive and learning impairments in these mice (Fig. 5k, l). These results suggest that TREM-1 knockout in endothelial cells can alleviate BBB disruption and brain function impairment in sepsis. The inhibition of TREM-1 remains a promising target for the development of therapies for sepsis.

Inhibition of TREM-1 prevents degradation of the BBB through the PI3K/Akt signaling pathway, thereby alleviating brain injury in sepsis

Previous studies have shown that PI3K/Akt signaling plays an antineuroinflammatory role in neurological diseases [42]. Our RNA-sequencing results also revealed that PI3K/Akt signaling may be involved in the pathogenesis of sepsis-induced disruption of the BBB (Figs. 2n and 3s). We further investigated whether the inhibition of TREM-1 alleviates disruption of the BBB through the PI3K/Akt signaling pathway, thereby ameliorating sepsis-induced brain injury. After the behavioral tests, Western blot analysis of PI3K/Akt pathway-related proteins in brain endothelial cells was performed to determine whether TREM-1 knockout in mouse brain endothelial cells triggers changes in the PI3K/Akt signaling pathway. Compared with the sham operation, the CLP operation significantly reduced the levels of PI3K and p-Akt, while the protein expression of PI3K and p-Akt increased after TREM-1 knockout in cerebral endothelial cells (Fig. 6a, b). The results of qRT−PCR revealed that the mRNA expression level of PI3K in the CLP group was significantly lower than that in the control group and that the mRNA expression level of PI3K in the TREM-1 knockout group was increased (Fig. 6c). Furthermore, in the human iPSC-derived BBB model, we used LY294002, a PI3K antagonist, to determine whether the PI3K/Akt signaling pathway is involved in the ability of TREM-1 inhibition to slow BBB disruption and brain injury in sepsis. After adding LY294002, we observed decreased expression of PI3K and p-Akt in endothelial cells within the cellular model (Fig. 7a), confirming the inhibitory effect of LY294002 on the PI3K pathway. TREM-1 knockdown has a protective effect on the integrity of the BBB. However, after the addition of LY294002, which inhibits PI3K, the TEER value of the model was reduced to approximately 430 $\Omega \cdot cm^2$, and the barrier integrity was reduced (Fig. 7b). The permeability experiments also revealed that TREM-1 knockout reduced the permeability of the BBB model, and the addition of LY294002 to inhibit PI3K increased the permeability of the model (Fig. 7c). These results indicated that the original protective effect of TREM-1 inhibition on the BBB was abolished by the addition of the PI3K inhibitor LY294002. These findings suggest that the PI3K/Akt pathway is involved in the protective effect of TREM-1 inhibition on the BBB. Furthermore, we conducted relevant animal experiments. After administering LY294002 to mice, we collected mouse brain endothelial cells and performed western blotting to assess the expression of key molecules in the PI3K pathway. The results demonstrated that LY294002 indeed reduced the expression of PI3K and phosphorylated Akt (p-Akt) in brain endothelial cells (Fig. 7d, e). In TREM-1 knockout mice, disruption of the BBB was alleviated after CLP, whereas LY294002 aggravated disruption of the BBB. These findings indicated that inhibition of the PI3K pathway could significantly eliminate the protective effect of TREM-1 knockout on the BBB in mice (Fig. 7f). Behavioral experiments in mice also demonstrated that PI3K inhibition partially counteracted the protective effect of TREM-1 knockout on brain function. In the novel object recognition test, compared with control mice, TREM-1 knockout mice, which also underwent

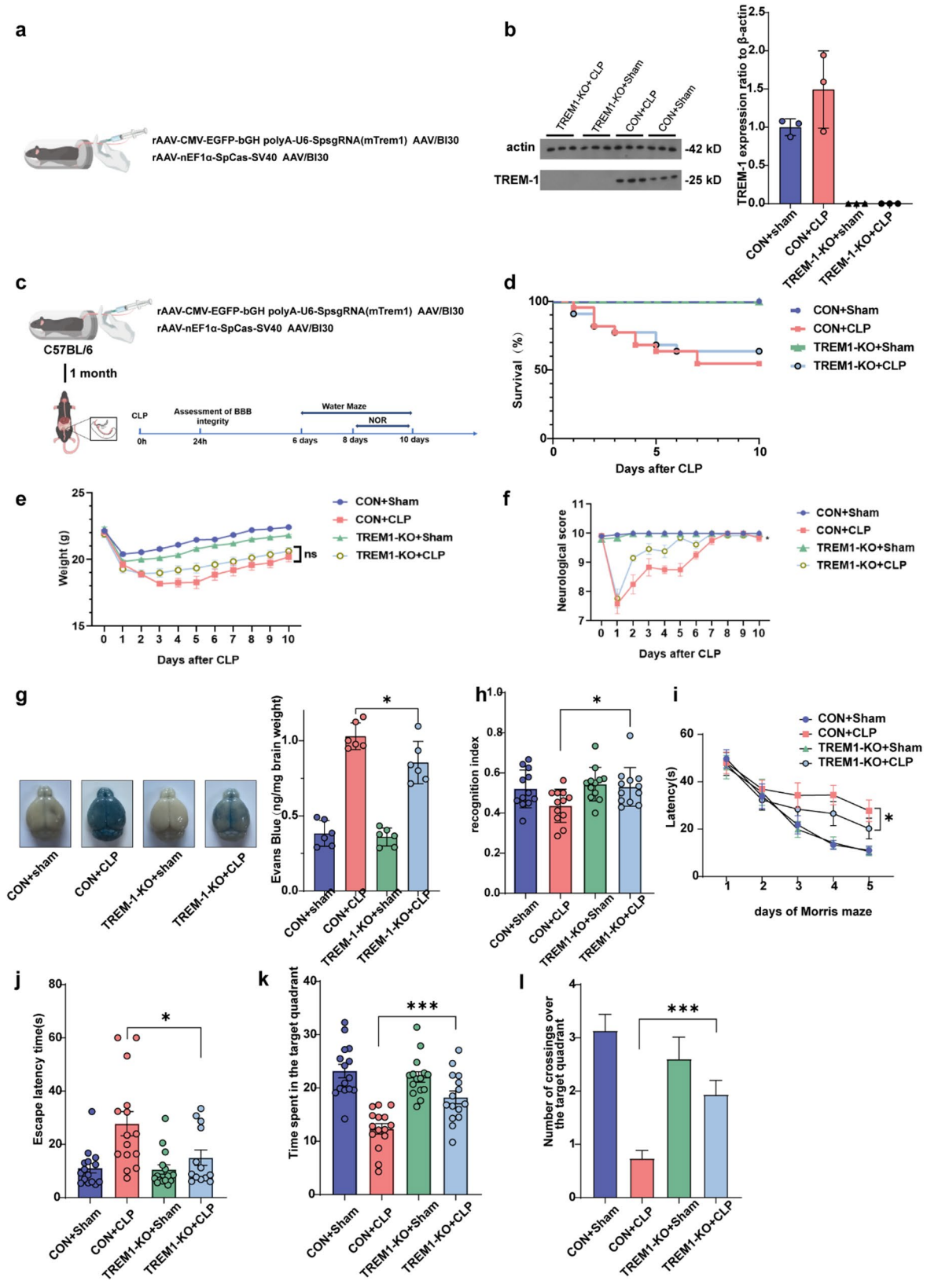

Fig. 5 (See legend on next page.)

(See figure on previous page.)

Fig. 5 TREM-1 knockout in endothelial cells alleviates cognitive impairment in a CLP mouse model. **a**, Schematic representation of rAAV vectors expressing control (CTL) or TREM-1 sgRNA. **b**, Western blot analysis of TREM-1 expression in mouse brain endothelial cells after injection of the TREM-1 sgRNA. **c**, Schematic illustration of the experimental design. **d**, Mortality of mice in the CON + sham ($n = 20$ mice), CON + CLP ($n = 22$ mice), TREM-1 sgRNA + sham ($n = 20$ mice), and TREM-1 sgRNA + CLP ($n = 22$ mice) groups within 10 days after the operation. **e**, Changes in the body weights of mice in the CON + sham ($n = 20$ mice), CON + CLP ($n = 12$ mice), TREM-1 sgRNA + sham ($n = 20$ mice), and TREM-1 sgRNA + CLP ($n = 14$ mice) groups within 10 days after the operation. **f**, Neurological scores of mice in the CON + sham ($n = 20$ mice), CON + CLP ($n = 12$ mice), TREM-1 sg RNA + sham ($n = 20$ mice), and TREM-1 sgRNA + CLP ($n = 14$ mice) groups within 10 days after surgery. **g**, EB leakage in the CON + sham ($n = 20$ mice), CON + CLP ($n = 12$ mice), TREM-1 sg RNA + sham ($n = 20$ mice), and TREM-1 sgRNA + CLP ($n = 14$ mice) groups 24 h after surgery. **h**, Recognition index of mice in the CON + sham, CON + CLP, TREM-1 sg RNA + sham, and TREM-1 sgRNA + CLP, $n = 12$ mice per group. **i-j**, Latency time of mice in the CON + sham, CON + CLP, TREM-1 sg RNA + sham, and TREM-1 sgRNA + CLP, $n = 15$ mice per group. **k**, Time spent in the target quadrant by mice in the CON + sham, CON + CLP, TREM-1 sg RNA + sham, and TREM-1 sgRNA + CLP, $n = 15$ mice per group. **l**, Number of crossing over the platform in the CON + sham, CON + CLP, TREM-1 sg RNA + sham, and TREM-1 sgRNA + CLP, $n = 15$ mice per group. The data are presented as the means ± SEMs. ns, not significant, $^{*}P < 0.05$, $^{**}P < 0.01$, $^{***}P < 0.001$, Student's t test

CLP surgery, presented an increased recognition index, demonstrating the protective effect of TREM-1 knockout on cognitive and memory abilities. However, after the injection of LY294002, the recognition index of the mice decreased (Fig. 7g). In the water maze test, we found that TREM-1 knockout mice took a shorter amount of time to find the platform, moved in the target quadrant for a longer period of time, and crossed the target quadrant more times, indicating that the mice had improved cognitive function. However, inhibition of PI3K by LY294002 resulted in poor performance in the water maze (Fig. 7h-j). These findings suggest that the PI3K/Akt pathway is involved in the protective effect of TREM-1 inhibition on brain function and that the inhibition of PI3K can partially eliminate the protective effect of TREM-1 knockout on cognition and memory ability.

Discussion

Brain dysfunction occurs during the onset of sepsis. However, many patients with sepsis still experience long-term cognitive impairment after discharge, which affects memory, attention, verbal fluency, and executive ability [43]. Autopsy studies have shown that the damage to the nervous system caused by sepsis is profound, and ischemia can be observed in several brain regions, including the hippocampus, amygdala, and hypothalamus [13]. Owing to the complex pathophysiological features of sepsis-induced brain injury, there are currently no specific medical treatments for this disease [44]. BBB dysfunction plays an important role in the pathophysiology of sepsis and SAE. The disruption of the BBB enables toxic substances to enter the brain, which leads to changes in the structure and function of the brain and induces brain inflammation [9]. After the BBB is disrupted, the CNS becomes very vulnerable to neurotoxic factors such as free radicals, inflammatory mediators, and plasma and intravascular proteins [13, 45]. In the present study, we found that endothelial cells expressing TREM-1 mediated sepsis-induced BBB disruption and cognitive impairment via the PI3K/Akt pathway. The addition of serum from sepsis patients to the BBB cell model reduced the integrity of the cell monolayer. The CLP model septic mice also showed disruption of the hemorrhagic brain barrier and impaired brain function.

There are many obstacles to developing effective treatments for sepsis, such as poor translation between human disease and animal models, heterogeneity of patient samples selected in clinical trials, and variation in disease etiology. The establishment of normal human-sourced iPSC-derived endothelial cells, pericytes, and astrocytes as in vitro cell models of the BBB paves the way for the study of BBB dysfunction. In vitro human iPSC-derived BBB models have been established using different differentiation protocols [25, 46–48] and can be used to study BBB disorders in a variety of diseases, such as Alzheimer's disease and multiple sclerosis [49, 50]. This encouraged us to generate human iPSCs using skin samples collected from healthy people to construct BBB models and to simulate sepsis by adding serum from septic patients to the model cells to explore sepsis-induced BBB dysfunction, which may reveal a pathological process that is not fully understood.

To investigate the underlying mechanisms of sepsis and associated validation responses, several experimental animal models have been developed, all of which attempt to mimic the pathophysiological changes typical of septic patients [51]. CLP is widely used to establish an experimental sepsis model, and the CLP sepsis model is currently considered the gold standard for sepsis research [52–54]. The establishment of a sepsis model via CLP leads to an increase in the brain water content and disruption of the BBB. This model can be used to simulate the pathology of clinical septic patients [55]. In our study, a CLP sepsis model was established, and the levels of inflammatory factors in the serum of model mice were measured. The levels of IL-1β and IL-6 were increased, which was consistent with previous studies [56]. In CLP, the cecal ligation distance is a major determinant of surgical severity and mortality. In addition, the size of the puncture needle, the number of punctures, and fluid resuscitation all have an impact on the surgical effect [52]. Therefore, performing the CLP procedure with high consistency and reproducibility is particularly important. Our experiment strictly controlled the above operations

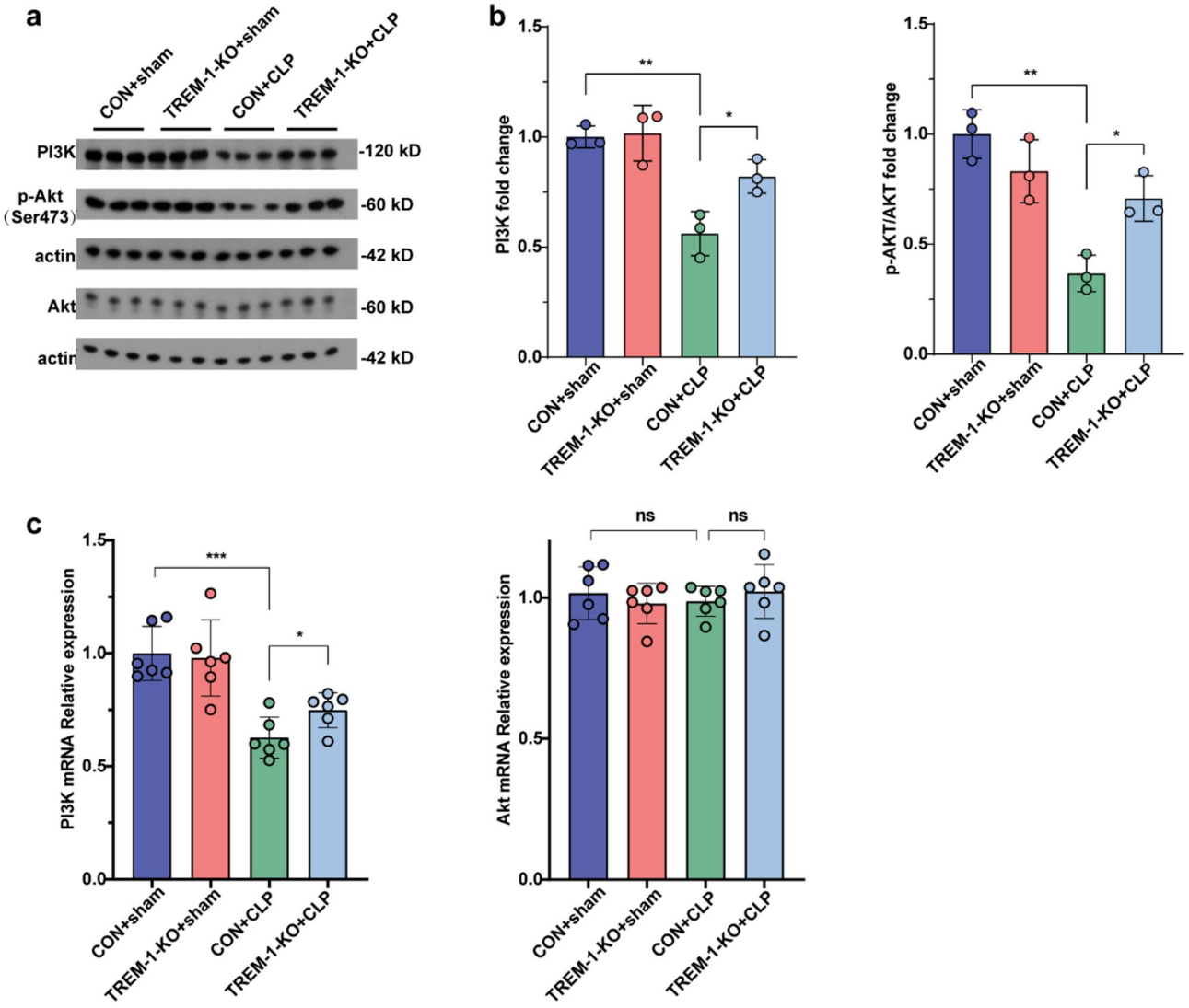

Fig. 6 Changes in the protein expression in the PI3K/AKT signaling pathway in mouse brain endothelial cells. **a**, The protein levels of PI3K, AKT, and p-AKT were measured by Western blotting. β-actin served as a reference protein. **b**, The expression ratios of the PI3K/β-actin and p-Akt/Akt proteins were quantified via ImageJ software. **c**, The expression levels of PI3K and AKT were measured via qRT–PCR. $n = 3$ per group for b. $n = 6$ per group for c. The data are presented as the means ± SEMs. ns, not significant, $^{*}P < 0.05$, $^{**}P < 0.01$, $^{***}P < 0.001$, One-way ANOVA

to ensure the consistency of the CLP surgery. In addition, we also utilized an in vitro human iPSC-derived BBB model, which to some extent complemented the animal model.

The TREM family includes at least 5 distinct receptors that share sequence homology. Among them, Trem-1 plays an important role in the process of inflammation-related diseases [57]. LPS can activate TLR4 and further amplify the inflammatory response. LR12, a clinically available TREM-1 inhibitory peptide, can prevent the binding of TREM-1 ligands, specifically inhibiting TREM-1 and blocking the amplification of inflammation [58]. However, the use of TREM-1 inhibitory peptides such as LR12 has limitations, and the "endothelial protection" observed in vivo may simply be the result of systemic inflammation and reduced activation of inflammatory cells [58]. To eliminate this concern, we used rAAV vectors to target brain endothelial cells and deliver sgRNA for TREM-1 knockdown. This method ensured the normal expression of TREM-1 in other non-endothelial cells. Using animal experiments, we found that depletion of TREM-1 in brain endothelial cells protected against the disruption of the BBB and cognitive impairment caused by CLP in mice, suggesting that endothelial TREM-1 mediates sepsis-associated brain damage.

The PI3K-AKT signaling pathway regulates signal transduction; cell proliferation, apoptosis, and metabolism; and other biological processes. Accumulating evidence suggests that the PI3K/Akt pathway plays a neuroprotective role in a variety of diseases, which provides

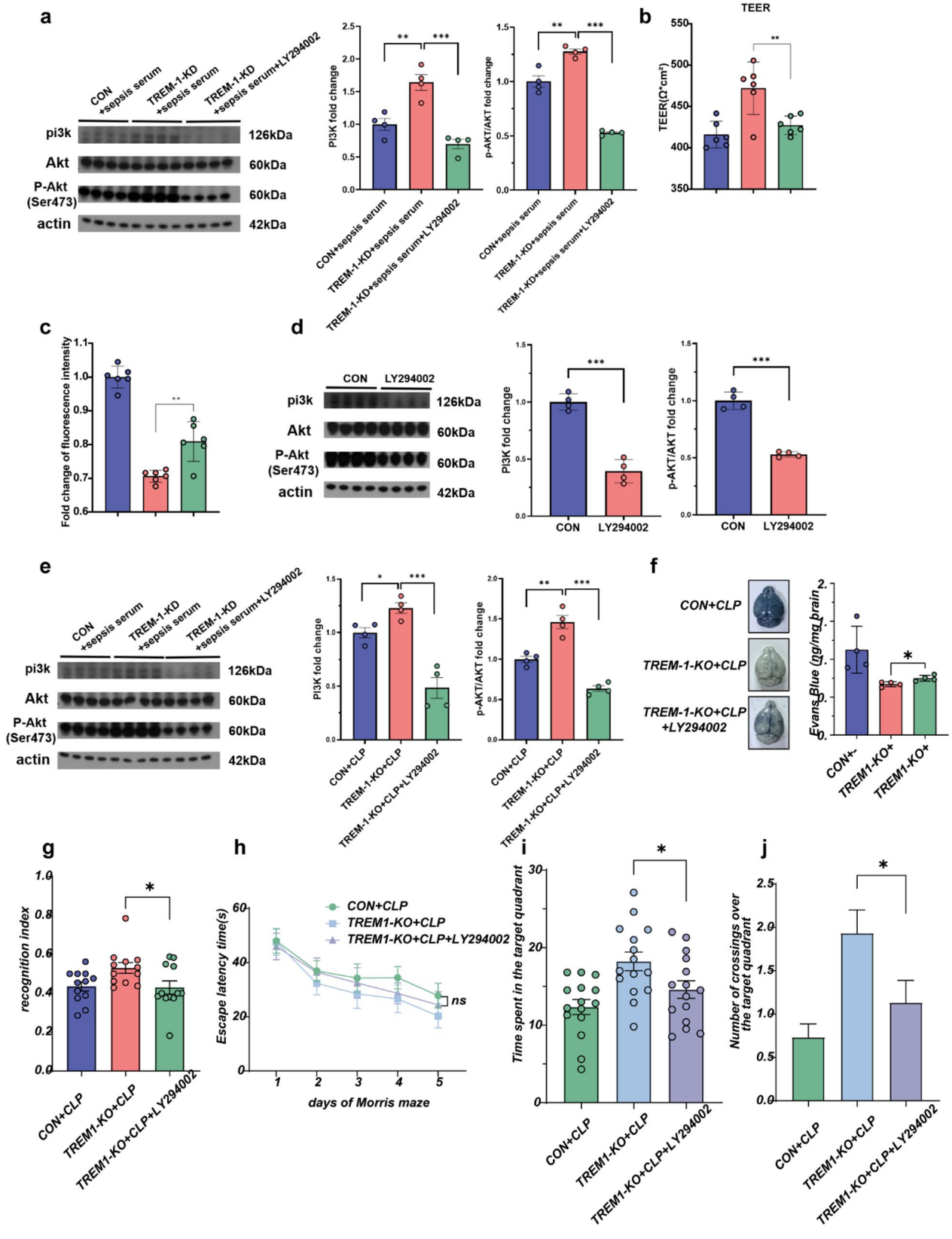

Fig. 7 (See legend on next page.)

(See figure on previous page.)

Fig. 7 Inhibition of PI3K partially abolished the protective effect of TREM-1 knockout on the BBB and cognitive function. **a**, The protein levels of PI3K, AKT, and p-AKT were measured by Western blotting. β-actin served as a reference protein. **b**, TEER values of the BBB models in the CON + septic serum, TREM-1-KD + septic serum, and TREM-1-KD + septic serum + LY294002 groups. **c**, Permeability of fluorescently labeled dextran (10 kDa) in the CON + septic serum, TREM-1-KD + septic serum, and TREM-1-KD + septic serum + LY294002 groups. **d**, Representative western blot analysis of PI3K, Akt, and p-Akt expression in brain endothelial cells isolated from control mice and LY294002-treated mice. **e**, Western blot analysis of PI3K/Akt pathway components in brain endothelial cells from CON + CLP, TREM-1-KO + CLP and TREM-1-KO + CLP + LY294002 groups. **f**, EB leakage in the CON + septic serum, TREM-1-KO + septic serum, and TREM-1-KO + septic serum + LY294002 groups. **g**, Recognition indices of mice in the CON + septic serum, TREM-1-KO + septic serum, and TREM-1-KO + septic serum + LY294002 groups. **h**, Latency time of mice in the CON + septic serum, TREM-1-KD + septic serum, and TREM-1-KD + septic serum + LY294002 groups. **i**, Time spent in the target quadrant by mice in the CON + septic serum, TREM-1-KD + septic serum, and TREM-1-KD + septic serum + LY294002 groups. **j**, Times at which the mice crossed the platform in the CON + septic serum, TREM-1-KD + septic serum, and TREM-1-KD + septic serum + LY294002 groups. $n = 4$ per group for a, d-f. $n = 6$ per group for b-c. $n = 12$ per group for g, $n = 15$ per group for h-j. The data are presented as the means ± SEMs. ns, not significant, $^{*}P < 0.05$, $^{**}P < 0.01$, $^{***}P < 0.001$

an effective resource for the discovery of potential therapeutic drugs [59]. The PI3K/Akt signaling pathway is thought to play an important role in sepsis [60]. Studies have shown that activation of the PI3K/Akt pathway negatively regulates the nuclear factor-κB (NF-κB) activation pathway, suppresses proinflammatory responses, and improves cardiac function and prolongs survival time in mice with sepsis [22, 61, 62]. Our results indicate that sepsis leads to decreased levels of PI3K and phosphorylated AKT. However, TREM-1 knockdown or knockout significantly increased the levels of phosphorylated AKT, indicating that TREM1 is involved in the disruption of the BBB during sepsis and may exert its effects through PI3K/AKT pathway. In this study, LY294002, a PI3K antagonist, was used to examine the effect of PI3K inhibition on cognitive behavior in septic mice with cerebral endothelial cell-specific TREM-1 knockout. PI3K inhibition abolished the protective effect of TREM-1 knockout on the BBB and brain function. The regulatory interplay between TREM-1 and the PI3K/Akt pathway involves multi-step cascades. Existing studies confirm that PI3K/Akt pathway activation can suppress pro-inflammatory responses by negatively regulating the nuclear factor-κB (NF-κB) activation pathway, improving cardiac function and extending survival in septic mice [22, 61, 62]. Preclinical evidence indicates that PI3Kα-specific inhibitors (e.g., Alpelisib) targeting the p110α mutant significantly enhance therapeutic specificity in breast cancer [63], suggesting that endothelium-restricted PI3Kα inhibitors may represent optimized therapeutic strategies for sepsis management [64]. Although the PI3K/Akt pathway is one of the downstream pathways of TREM-1, the exact mechanism by which this signaling pathway contributes to the pathophysiological process of TREM-1 needs to be further investigated.

There are several limitations in our study. First, the cells used to construct the BBB model were derived from healthy individuals, and the serum of patients or healthy individuals was added to simulate the sepsis group or control group. Considering that there may be a genetic component in the development of sepsis, iPSC-derived BBB models established using cells derived from sepsis patients should also be established for comparison with normal controls and for further studies. Second, only male mice were used in the animal experiments in this study, whereas epidemiological studies have shown that young women have better prognoses and clinical outcomes than men do in with the context of sepsis [65]. Additional studies on the role of TREM-1 in sepsis-induced BBB disruption in female mice may provide further evidence of its function in sepsis. Finally, the molecular and cellular mechanisms through which TREM-1 induces BBB disruption and cognitive impairment during sepsis need to be further investigated, especially its role in regulating the PI3K/Akt pathway.

In summary, our findings suggest that endothelial TREM-1 mediates BBB disruption and cognitive impairment in sepsis. TREM-1 inhibition can alleviate BBB disruption and cognitive dysfunction through the PI3K/Akt pathway. TREM-1 inhibition can be used as a treatment option for sepsis. However, the pathogenesis of sepsis is complex, and future studies should further explore the signaling mechanisms of TREM-1 in endothelial cells and the interactions between TREM-1 and the PI3K/Akt pathways and other signaling pathways.

Conclusions

Our study revealed the mechanism of BBB disruption during sepsis. In both the human iPSC-derived BBB model and the mouse model of sepsis induced by CLP surgery, endothelial TREM-1 was involved in the disruption of the BBB. CLP treatment disrupted the BBB and impaired cognitive ability in mice. We demonstrated that the inhibition of TREM-1 improves the function of the BBB and alleviates cognitive impairment through the PI3K/Akt pathway. Our findings suggest that TREM-1 and PI3K/Akt pathway members may be promising therapeutic targets for the treatment of sepsis.

Abbreviations

BBB	Blood-brain barrier
CLP	Cecal ligation and puncture
CNS	Central nervous system
FITC	Fluorescein isothiocyanate
GFAP	Glial fibrillary acidic protein
GLUT1	glucose transporter type 1

IL-1β	Interleukin-1 beta
IL-6	Interleukin-6
KD	Knock down
KO	Knock out
LPS	Lipopolysaccharide
LRP-1	Low-density lipoprotein receptor-related protein-1
MWM	Morris water maze
NPC	Neural progenitor cell
PECAM-1/CD31	platelet endothelial cell adhesion molecule-1
PI3K	Phosphatidylin-ositol-3-kinase
SAE	Sepsis-associated encephalopathy
TEER	Transepithelial/transendothelial electrical resistance
TREM-1	Triggering receptor expressed on myeloid cell-1
ZO-1	zonula occludens-1
α-SMA	Alpha smooth muscle actin

Supplementary Information

The online version contains supplementary material available at https://doi.org/10.1186/s12974-025-03469-5.

Supplementary Material 1

Supplementary Material 2

Author contributions

Y.S., W.Z., T.S., L.H., M.Q., and Q.W. performed the research; Y.S. and L.H. analyzed the experimental data; Y.S. wrote the main manuscript text. Q.X., Y.L., and J.X. supervised the laboratory experiments and substantively revised the manuscript; and all other authors reviewed and commented on the manuscript.

Funding

This work was supported by research grants from STI2030-Major Projects (2022ZD0211701, 2021ZD0203001), the CAMS Innovation Fund for Medical Sciences (2021-I2M-1-020), the National High Level Hospital Clinical Research Funding (2022-PUMCH-B-109), Special Research Fund for Central Universities, Peking Union Medical College (3332024120), and the Fundamental Research Funds for the Central Universities, Peking Union Medical College.

Data availability

Raw data are available upon reasonable request from the corresponding authors.

Declarations

Ethics approval and consent to participate

All animals were raised and handled in accordance with the protocol approved by the institutional review board of the IBMS & Peking Union Medical College and were conducted according to the Beijing Administration Office of Laboratory Animals guidelines for the care and use of laboratory animals. The work involving human serum samples in this article was approved by the Ethics Institutional Review Board of Peking Union Medical College Hospital (PUMCH) (serial number: ZS-2165).

Consent for publication

All authors agreed to the content of this manuscript prior to submission.

Competing interests

The authors declare no competing interests.

Received: 24 January 2025 / Accepted: 15 May 2025
Published online: 27 May 2025

References

1. Rudd KE, Johnson SC, Agesa KM, Shackelford KA, Tsoi D, Kievlan DR, et al. Global, regional, and National sepsis incidence and mortality, 1990–2017: analysis for the global burden of disease study. Lancet. 2020;395:200–11.
2. Fleischmann C, Scherag A, Adhikari NKJ, Hartog CS, Tsaganos T, Schlattmann P, et al. Assessment of global incidence and mortality of Hospital-treated sepsis. Current estimates and limitations. Am J Respir Crit Care Med. 2016;193:259–72.
3. Xin Y, Tian M, Deng S, Li J, Yang M, Gao J, et al. The key drivers of brain injury by systemic inflammatory responses after sepsis: microglia and neuroinflammation. Mol Neurobiol. 2023;60:1369–90.
4. Barichello T, Giridharan VV, Catalão CHR, Ritter C, Dal-Pizzol F. Neurochemical effects of sepsis on the brain. Clin Sci (Lond). 2023;137:401–14.
5. Mazeraud A, Righy C, Bouchereau E, Benghanem S, Bozza FA, Sharshar T. Septic-Associated encephalopathy: a comprehensive review. Neurotherapeutics. 2020;17:392–403.
6. Zhang Y-Y, Ning B-T. Signaling pathways and intervention therapies in sepsis. Signal Transduct Target Ther. 2021;6:407.
7. Nwafor DC, Brichacek AL, Mohammad AS, Griffith J, Lucke-Wold BP, Benkovic SA, et al. Targeting the Blood-Brain barrier to prevent Sepsis-Associated cognitive impairment. J Cent Nerv Syst Dis. 2019;11:1179573519840652.
8. Towner RA, Saunders D, Smith N, Towler W, Cruz M, Do S, et al. Assessing long-term neuroinflammatory responses to encephalopathy using MRI approaches in a rat endotoxemia model. GeroScience. 2018;40:49–60.
9. Obermeier B, Daneman R, Ransohoff RM. Development, maintenance and disruption of the blood-brain barrier. Nat Med. 2013;19:1584–96.
10. Weksler BB, Subileau EA, Perrière N, Charneau P, Holloway K, Leveque M, et al. Blood-brain barrier-specific properties of a human adult brain endothelial cell line. FASEB J. 2005;19:1872–4.
11. Abbott NJ, Rönnbäck L, Hansson E. Astrocyte-endothelial interactions at the blood-brain barrier. Nat Rev Neurosci. 2006;7:41–53.
12. Ballabh P, Braun A, Nedergaard M. The blood-brain barrier: an overview: structure, regulation, and clinical implications. Neurobiol Dis. 2004;16:1–13.
13. Gao Q, Hernandes MS. Sepsis-Associated encephalopathy and Blood-Brain barrier dysfunction. Inflammation. 2021;44:2143–50.
14. Sweeney MD, Zhao Z, Montagne A, Nelson AR, Zlokovic BV. Blood-Brain barrier: from physiology to disease and back. Physiol Rev. 2019;99:21–78.
15. Erikson K, Tuominen H, Vakkala M, Liisanantti JH, Karttunen T, Syrjälä H, et al. Brain tight junction protein expression in sepsis in an autopsy series. Crit Care. 2020;24:385.
16. Huang X, Wei P, Fang C, Yu M, Yang S, Qiu L et al. Compromised endothelial Wnt/β-catenin signaling mediates the blood-brain barrier disruption and leads to neuroinflammation in endotoxemia. 2024.
17. Boufenzer A, Carrasco K, Jolly L, Brustolin B, Di-Pillo E, Derive M, et al. Potentiation of NETs release is novel characteristic of TREM-1 activation and the Pharmacological Inhibition of TREM-1 could prevent from the deleterious consequences of NETs release in sepsis. Cell Mol Immunol. 2021;18:452–60.
18. Gibot S, Jolly L, Lemarié J, Carrasco K, Derive M, Boufenzer A. Triggering receptor expressed on myeloid cells-1 inhibitor targeted to endothelium decreases cell activation. Front Immunol. 2019;10:2314.
19. Bouchon A, Dietrich J, Colonna M. Cutting edge: inflammatory responses can be triggered by TREM-1, a novel receptor expressed on neutrophils and monocytes. J Immunol. 2000;164:4991–5.
20. Kung C-T, Su C-M, Hsiao S-Y, Chen F-C, Lai Y-R, Huang C-C, et al. The prognostic value of serum soluble TREM-1 on outcome in adult patients with Sepsis. Diagnostics (Basel). 2021;11:1979.
21. Siskind S, Brenner M, Wang P. TREM-1 modulation strategies for Sepsis. Front Immunol. 2022;13:907387.
22. Jiang S, Zhu W, Li C, Zhang X, Lu T, Ding Z, et al. α-Lipoic acid attenuates LPS-induced cardiac dysfunction through a PI3K/Akt-dependent mechanism. Int Immunopharmacol. 2013;16:100–7.
23. Tu X-K, Zhang H-B, Shi S-S, Liang R-S, Wang C-H, Chen C-M, et al. 5-LOX inhibitor Zileuton reduces inflammatory reaction and ischemic brain damage through the activation of PI3K/Akt signaling pathway. Neurochem Res. 2016;41:2779–87.
24. de Oliveira Matos A, Dos Santos Dantas PH, Figueira Marques Silva-Sales M, Sales-Campos H. The role of the triggering receptor expressed on myeloid cells-1 (TREM-1) in non-bacterial infections. Crit Rev Microbiol. 2020;46:237–52.
25. King NE, Courtney J-M, Brown LS, Fortune AJ, Blackburn NB, Fletcher JL, et al. Induced pluripotent stem cell derived pericytes respond to mediators of proliferation and contractility. Stem Cell Res Ther. 2024;15:59.
26. Faal T, Phan DTT, Davtyan H, Scarfone VM, Varady E, Blurton-Jones M, et al. Induction of mesoderm and neural Crest-Derived pericytes from human pluripotent stem cells to study Blood-Brain barrier interactions. Stem Cell Rep. 2019;12:451–60.

27. Vorhees CV, Williams MT. Morris water maze: procedures for assessing Spatial and related forms of learning and memory. Nat Protoc. 2006;1:848–58.
28. Lueptow LM. Novel object recognition test for the investigation of learning and memory in mice. J Vis Exp. 2017;55718.
29. Chow BW, Gu C. The molecular constituents of the blood-brain barrier. Trends Neurosci. 2015;38:598–608.
30. Armulik A, Genové G, Mäe M, Nisancioglu MH, Wallgard E, Niaudet C, et al. Pericytes regulate the blood-brain barrier. Nature. 2010;468:557–61.
31. Srinivasan B, Kolli AR, Esch MB, Abaci HE, Shuler ML, Hickman JJ. TEER measurement techniques for in vitro barrier model systems. J Lab Autom. 2015;20:107–26.
32. Ozgür B, Puris E, Brachner A, Appelt-Menzel A, Oerter S, Balzer V, et al. Characterization of an iPSC-based barrier model for blood-brain barrier investigations using the SBAD0201 stem cell line. Fluids Barriers CNS. 2023;20:96.
33. Alnaqbi N, Mohammad MG, Hamoudi R, Mabondzo A, Harati R. Molecular heterogeneity of the brain endothelium. Curr Issues Mol Biol. 2023;45:3462–78.
34. Deng P, Tang N, Li L, Zou G, Xu Y, Liu Z. Diagnostic value of combined detection of IL-1β, IL-6, and TNF-α for sepsis-induced cardiomyopathy. Med Clin (Barc). 2022;158:413–7.
35. Kurt ANC, Aygun AD, Godekmerdan A, Kurt A, Dogan Y, Yilmaz E. Serum IL-1beta, IL-6, IL-8, and TNF-alpha levels in early diagnosis and management of neonatal sepsis. Mediators Inflamm. 2007;2007:31397.
36. Giridharan VV, Generoso JS, Lence L, Candiotto G, Streck E, Petronilho F, et al. A crosstalk between gut and brain in sepsis-induced cognitive decline. J Neuroinflammation. 2022;19:114.
37. Li Z, Zhang F, Sun M, Liu J, Zhao L, Liu S, et al. The modulatory effects of gut microbes and metabolites on blood-brain barrier integrity and brain function in sepsis-associated encephalopathy. PeerJ. 2023;11:e15122.
38. Yang Y, Yun D, Dong B, Geng Y, Wan Y. VIP alleviates sepsis-induced cognitive dysfunction as the TLR-4/NF-κB signaling pathway is inhibited in the hippocampus of rats. J Mol Histol. 2022;53:369–77.
39. Zhang C, Kan X, Zhang B, Ni H, Shao J. The role of triggering receptor expressed on myeloid cells-1 (TREM-1) in central nervous system diseases. Mol Brain. 2022;15:84.
40. Chen Y, Mao L, Liu S, Huang S, Lin Q, Zeng M et al. The role of TREM-1 in septic myocardial pyroptosis and septic cardiomyopathy in vitro and in vivo. J Cell Physiol. 2024;e31445.
41. Krolak T, Chan KY, Kaplan L, Huang Q, Wu J, Zheng Q et al. A High-Efficiency AAV for endothelial cell transduction throughout the central nervous system. 2022.
42. Fu A, Qiao F, Feng H, Luo Q. Inhibition of TREM-1 ameliorates Lipopolysaccharide-induced depressive-like behaviors by alleviating neuroinflammation in the PFC via PI3K/Akt signaling pathway. Behav Brain Res. 2023;449:114464.
43. Ji M-H, Gao Y-Z, Shi C-N, Wu X-M, Yang J-J. Acute and long-term cognitive impairment following sepsis: mechanism and prevention. Expert Review of Neurotherapeutics [Internet]. 2023 [cited 2024 Nov 19]; Available from: https://www.tandfonline.com/doi/abs/https://doi.org/10.1080/14737175.2023.2250917
44. Czempik PF, Pluta MP, Krzych ŁJ. Sepsis-Associated brain dysfunction: A review of current literature. Int J Environ Res Public Health. 2020;17:5852.
45. Handa O, Stephen J, Cepinskas G. Role of endothelial nitric oxide synthase-derived nitric oxide in activation and dysfunction of cerebrovascular endothelial cells during early onsets of sepsis. Am J Physiol Heart Circ Physiol. 2008;295:H1712–1719.
46. Nishihara H, Gastfriend BD, Soldati S, Perriot S, Mathias A, Sano Y et al. Advancing human induced pluripotent stem cell-derived blood-brain barrier models for studying immune cell interactions.
47. Pilz RA, Skowronek D, Mellinger L, Bekeschus S, Felbor U, Rath M. Endothelial differentiation of CCM1 knockout iPSCs triggers the establishment of a specific gene expression signature. Int J Mol Sci. 2023;24:3993.
48. Lee C, Frew J, Weilinger NL, Wendt S, Cai W, Sorrentino S, et al. hiPSC-derived GRN-deficient astrocytes delay spiking activity of developing neurons. Neurobiol Dis. 2023;181:106124.
49. Blanchard JW, Bula M, Davila-Velderrain J, Akay LA, Zhu L, Frank A, et al. Reconstruction of the human blood-brain barrier in vitro reveals a pathogenic mechanism of APOE4 in pericytes. Nat Med. 2020;26:952–63.
50. Nishihara H. Intrinsic blood–brain barrier dysfunction contributes to multiple sclerosis pathogenesis.
51. Rittirsch D, Huber-Lang MS, Flierl MA, Ward PA. Immunodesign of experimental sepsis by cecal ligation and puncture. Nat Protoc. 2009;4:31–6.
52. Rittirsch D, Hoesel LM, Ward PA. The disconnect between animal models of sepsis and human sepsis. J Leukoc Biol. 2007;81:137–43.
53. Remick DG, Newcomb DE, Bolgos GL, Call DR. Comparison of the mortality and inflammatory response of two models of sepsis: lipopolysaccharide vs. cecal ligation and puncture. Shock. 2000;13:110–6.
54. Ea D. Rodent models of intra-abdominal infection. Shock (Augusta, Ga) [Internet]. 2005 [cited 2024 Dec 26];24 Suppl 1. Available from: https://pubmed.ncbi.nlm.nih.gov/16374368/
55. Tang G, Yang H, Chen J, Shi M, Ge L, Ge X, et al. Metformin ameliorates sepsis-induced brain injury by inhibiting apoptosis, oxidative stress and neuroinflammation via the PI3K/Akt signaling pathway. Oncotarget. 2017;8:97977–89.
56. Reis PA, Alexandre PCB, D'Avila JC, Siqueira LD, Antunes B, Estato V, et al. Statins prevent cognitive impairment after sepsis by reverting neuroinflammation, and microcirculatory/endothelial dysfunction. Brain Behav Immun. 2017;60:293–303.
57. Klesney-Tait J, Turnbull IR, Colonna M. The TREM receptor family and signal integration. Nat Immunol. 2006;7:1266–73.
58. Jolly L, Carrasco K, Derive M, Lemarié J, Boufenzer A, Gibot S. Targeted endothelial gene deletion of triggering receptor expressed on myeloid cells-1 protects mice during septic shock. Cardiovasc Res. 2018;114:907–18.
59. Goyal A, Agrawal A, Verma A, Dubey N. The PI3K-AKT pathway: A plausible therapeutic target in Parkinson's disease. Exp Mol Pathol. 2023;129:104846.
60. Sun N, Wang H, Ma L, Lei P, Zhang Q. Ghrelin attenuates brain injury in septic mice via PI3K/Akt signaling activation. Brain Res Bull. 2016;124:278–85.
61. Zhou H, Qian J, Li C, Li J, Zhang X, Ding Z, et al. Attenuation of cardiac dysfunction by HSPA12B in endotoxin-induced sepsis in mice through a PI3K-dependent mechanism. Cardiovasc Res. 2011;89:109–18.
62. Williams DL, Ozment-Skelton T, Li C. Modulation of the phosphoinositide 3-kinase signaling pathway alters host response to sepsis, inflammation, and ischemia/reperfusion injury. Shock. 2006;25:432–9.
63. André F, Ciruelos E, Rubovszky G, Campone M, Loibl S, Rugo HS, et al. Alpelisib for PIK3CA-Mutated, hormone Receptor-Positive advanced breast Cancer. N Engl J Med. 2019;380:1929–40.
64. Vasan N, Toska E, Scaltriti M. Overview of the relevance of PI3K pathway in HR-positive breast cancer. Ann Oncol. 2019;30:x3–11.
65. Vo Q, Simon ZD, Park G, Nacionales DC, Gorski C, Barrios EL et al. Functional connectivity within sensorimotor cortical and striatal regions is regulated by sepsis in a sex-dependent manner. NeuroImage. 2025;120995.

Publisher's note